中國機械工程學刊第四十五卷第一期第 33~40 頁(民國一百一十三年)
Journal of the Chinese Society of Mechanical Engineers, Vol.45, No.1, pp 33~40 (2024)

Modal Analysis and Optimal Design of Spirally Corrugated Tubes

Chuang Pan**, Yuan-De Dai* and Qing-Qing Tang**

Keywords：spirally corrugated tube, modal analysis, natural frequency, amplitude, orthogonal test.

ABSTRACT

Spirally corrugated tube is a cost-effective option for efficient heat exchange due to its simple manufacturing and two-way heat transfer enhancement. To ensure the tube bundle structure can withstand vibrations, spirally corrugated tubes with equal inner diameters were chosen for analysis. Numerical simulations were conducted for modal analysis, studying the impact of start value, pitch, and corrugated depth on vibration characteristics. Results show that as the number of starts increases, the natural frequency initially decreases then increases, and the first-order maximum amplitude decreases. As pitch increases, the natural frequency decreases and the first-order maximum amplitude increases, while increasing corrugated depth decreases both. In low-frequency environments, heat exchange tubes are prone to resonance, causing fatigue failure. Therefore, the first-order natural frequency is used as the target parameter to optimize the design of the multi-start spirally corrugated tubes, and the structural parameters with the best vibration resistance are obtained.

1. INTRODUCTION

The shell-and-tube heat exchanger is one of the most widely used heat exchange equipment in the industrial field, and the heat exchange tube is one of its important components, which plays a decisive role in the heat exchange capacity of the heat exchanger (Bergles 1988; Guo et al., 2013). As an efficient heat exchange tube, the spiral corrugated tube has the advantages of simple manufacture, two-way heat transfer, and low pressure drop, which have been widely studied by relevant scholars (Yang et al., 2011; Navaei et al., 2015; Jin et al., 2016). For heat exchange tubes, heat transfer capacity is an important index to evaluate their performance, and the safetyand vibration resistance of the elements are the basis for determining whether they have practical engineering significance, which should be paid more attention to (Zhou et al., 2013; Hou et al., 2009). Due to the harsh working environment of the heat exchange tube, it is often impacted by cold and hot fluids, resulting in mechanical stress and thermal stress inside it, increasing the probability of fatigue failure (Ji et al., 2022). Generally, fatigue failure manifests itself as a fracture or damage to the tube bundle. Frequent failures not only increase the maintenance cost of the heat exchanger but also affect the normal operation of the whole machine (Ji et al., 2022; Wang and Lambert, 1996). Therefore, it is necessary to study the vibration characteristics of spiral bellows.

In recent years, many scholars have conducted in-depth research on tube bundle vibration. Ashley et al. (1950) studied the actual vibration problem of heat exchange tubes in power plants and nuclear reactors and established a finite element model and numerical method for the vibration problem of flow in tubes. Yan et al. (2010) applied the finite element method to the fluid-structure interaction of conical spiral tube bundles and established the vibration equation and element matrix of the tube. It is found that as the flow rate increases, the natural frequency of the tube bundle decreases, and the critical speed of vibration buckling is obtained. Lee et al. (2006) utilized the principles of fluid mechanics and Hamilton's principle, using transverse displacement, axial displacement, fluid pressure, and fluid velocity as dependent variables. A spectral element model representing the exact dynamic stiffness matrix of the tube bundle was established, and spectral dynamics analysis based on Fast Fourier Transform (FFT) was conducted to evaluate the accuracy of the present spectral element model. Ghadirian et al. (2022) derived the nonlinear motion equation of the system by using the extended Hamilton principle for systems, used the super convergent finite element method to discretize the

Paper Received May, 2023. Revised August, 2023. Accepted November, 2023. Author for Correspondence: Yuan-De Dai.

** Graduate Student, School of Advanced Manufacturing, Nanchang University, Nanchang 330031, China*

*** Associate Professor, School of Advanced Manufacturing, Nanchang University, Nanchang 330031, China*

nonlinear coupled partial differential equations, and numerically studied the nonlinear free vibration and fluid flow effects in the carbon nano-tube pipe system. The nonlinear free vibration law and stability conditions of carbon nano-tube pipes are obtained. Liu et al. (2021) performed nonlinear free vibration analysis on a shear deformable functionally graded material (FGM) tubes conveying fluid with immovable support conditions resting on a Pasternak-type foundation. Based on the Hamilton principle, the nonlinear frequency and amplitude-frequency responses of fluid-conveying FGM tubes under different boundary conditions are obtained. The effects of different types of boundary conditions and geometric and physical properties are analyzed. It is found that geometric and physical properties are crucial factors affecting the dynamic behavior of pipelines. By using the finite element software ANSYS CFX and ANSYS Mechanical, Jing et al. (2016) discussed the FSI analysis program of the gas-water two-phase flow cross-tube model with fixed ends and analyzed the dynamic behavior of the vibration caused by the internal flow under different two-phase flow velocities and different volume fractions. Wang et al. (2012) established a fluid-solid coupling model of the structural interaction between the fluid inside the tube line and the fluid outside the tube line by using the finite element software ADINA. The first six natural frequencies and main vibration modes under different ore transport volume concentrations and cross-sectional dimensions of the tube line were studied. It was found that the natural frequency and relative error of the tube line decreased with the increase in volume concentration and relative wall thickness. Li et al. (2019) studied the vibration of compressor tube lines under the interaction of tube line structure and gas flow in tube lines by combining simulation with experiment. The results show that the higher the pressure in the tube line, the greater the fluid-structure coupling vibration, and the coupling vibration not only occurs in the studied tube line but also propagates to the downstream tube line in the distance. Based on the fluid-solid coupling theory, Zhang et al. (2012) established the heat transfer tube model, conducted research on the weakening effect of fluid holes on fluid, and analyzed the natural frequencies of the heat transfer tubes under different fluid holes and fluid hole distances by numerical simulation. Fan et al. (2010) used the characteristic line method and the 4-equation model to numerically calculate the fluid-solid coupling vibration response of the water tube line. The influence of wave velocity on the numerical results and the influence of tube line structure damping on the vibration response of a water tube line are studied. The numerical results show that the influence of the structural damping of the tube line on the vibration response of the water tube line is more obvious than the friction between the tube wall and the liquid, and the structural damping of the tube line can attenuate the vibration of the system faster. Peng et al. (2015) also used the 4-equation model to establish the axial coupling vibration equations of the TBM hydraulic tube line under axial foundation vibration and analyzed the influence of foundation vibration and different structural parameters on fluid frequency domain response. At the same time, in order to reduce the influence of foundation vibration on fluid outlet parameters, the orthogonal experiment method is used to optimize the structure of the tube line. Qu et al. (2021) used Hamilton's principle to determine the stochastic vibration motion equation of a curved tube conveying fluid, taking into account the effects of fluid structure interaction and shear deformation. And the finite element method and random vibration discrete analysis method were used to solve it. The numerical calculation results indicate that different parameters have a significant impact on the dynamic characteristics of the bent tube. Wu et al. (2021) used fluid-solid coupling software to study the causes of vibration in subsea trees. The research shows that when the diameter and right angle are changed, the pressure of the flow field changes obviously, and the vibration of the long straight tube section is larger. The measures to reduce the vibration of the subsea tree tube line are put forward. The above research results show that the natural frequency is an important factor affecting the vibration of the tube bundle. The higher the natural frequency, the stronger the vibration resistance. In the low-frequency environment of the transverse and longitudinal impact of the fluid, the resonance phenomenon is easy to occur, resulting in fatigue failure. In order to improve the vibration resistance of the spiral bellows, its first-order natural frequency should be increased. The natural frequency is a unique property of the object that is only related to the material and shape of the object itself. Therefore, as an efficient heat exchange tube, the spirally corrugated tube's own structure (start value, pitch, and corrugated depth) not only affects its heat transfer performance but also affects its natural frequency.

Based on the finite element analysis method, the finite element model of multi-start spirally corrugated tubes with different corrugation depths and pitches is established. The effects of start value, pitch, and corrugation depth on the natural frequency and first-order maximum amplitude of spirally corrugated tubes are studied and compared with those of smooth tubes with equivalent inner diameters. Secondly, based on the orthogonal test method, the influence of the start value, corrugation depth ratio, and pitch ratio on the natural frequency of the spirally corrugated tube is studied, and the spirally corrugated tube with the best vibration resistance is obtained.

2. MODEL AND RELIABLE VERIFICATION

2.1 Geometric Model

In this paper, the copper multi-start spirally corrugated tube with the equivalent inner diameter is selected for simulation research. The basic parameters of the material (Wu et al., 2021): Poisson's ratio is 0.37, the elastic modulus is 110 GPa, and the density is 8900 kg/m^3. The length (L) of the spirally corrugated tube is 600 mm, and the wall thickness is 1.5 mm. Taking the three-start spirally corrugated tube as an example, the main structural parameters of the spirally corrugated tube are pitch p, corrugated depth e, spiral angle β, and inner diameter D_i, as shown in Fig. 1. The inner diameter is calculated as 4A/C, where A and C are the cross-sectional area and the wetting perimeter, respectively. The geometric parameters of this study are expressed in dimensionless form as pitch ratio p/D_i and ripple depth ratio e/D_i. According to the existing research on the flow and heat transfer in multi-start spirally corrugated tubes (Kongkaitpaiboon et al., 2019; Omidi et al., 2018), the range of parameters is determined as follows: the start value is 1-8, p/D_i is 1.5-3, and e/D_i is 0.05-0.20.

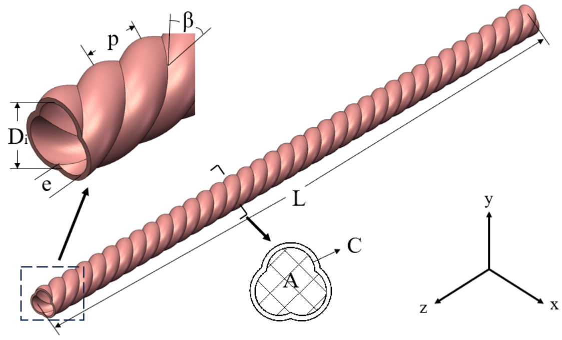

Fig. 1. Structural diagram of three-start spirally corrugated tube.

2.2 Grid Independence Verification

Based on the special structure of the spirally corrugated tubes, the surface mesh adopts the quadrilateral mesh, and the volume mesh adopts the hexahedral mesh. The mesh division is shown in Fig. 2. Taking the smooth tube without working fluid in the tube and the three-start spirally corrugated tubes (p/D_i=2.5; e/D_i=0.15) as examples to verify the grid independence, the results are shown in Table 1. When the number of grids is 7.06×10^5 and 1.29×10^6 respectively, the error is less than 5%, and the grid in the wall thickness direction is greater than three layers. Finally, the grid size is determined to be 0.8 mm.

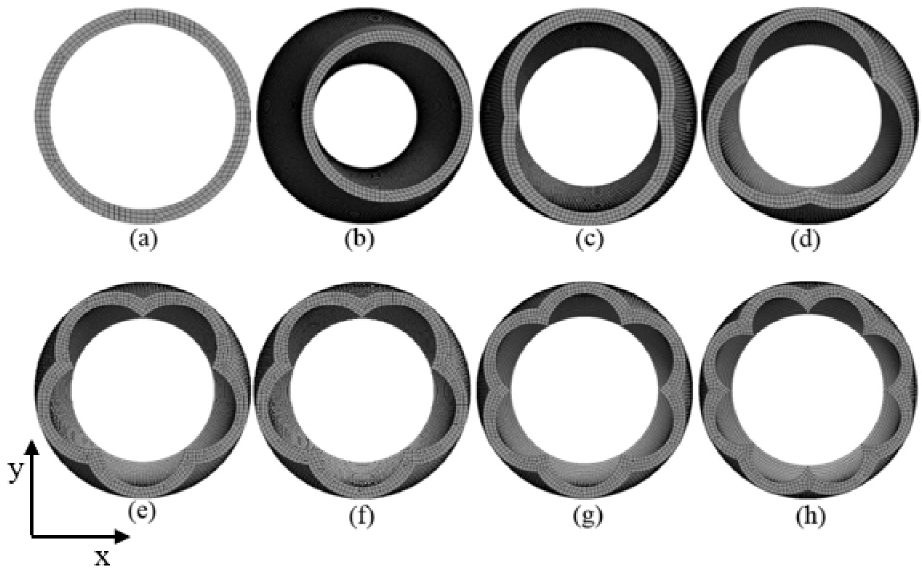

Fig. 2. Grid division model diagram: (a) Circular tube; (b) One-start; (c) Two-start; (d)Three-start; (e)Four-start; (f) Five-start; (g) Six-start; (h) Eight-start.

Table 1. Calculation results and errors of first Order natural frequency.

Circular tube			Three-start spirally corrugated tube		
Number of grids	First order natural frequency /Hz	Error	Number of grids	First order natural frequency /Hz	Error
312253	260.18	0.004%	581393	432.59	0.296%
706028	260.17	0	1292899	431.47	0.174%
1703023	260.17	——	2947302	430.96	——

3. RESULT ANALYSIS

3.1 Effect of Start Value

Fixed constraints are applied to both ends of the tube bundle, and the first nine natural frequencies of the 1-8 start spirally corrugated tubes (p/D_i=2.5 and e/D_i=0.15) are calculated. The results are shown in Fig. 3. The natural frequencies of the spirally corrugated tubes are lower than that of the circular tube. Due to the symmetry of the geometric structure of the tube bundle, the natural frequencies of the first and second orders, the third and fourth orders, and the fifth and sixth orders are equal to each other. With the increase in the number of starts, the mass of the spirally corrugated tube increases and the rotational moment increases. In addition, with the increase in the number of stars, the mass distribution of the spirally corrugated tube is more dispersed, resulting in the enhancement of the inertial effect, which is the resistance of the tube bundle vibration. These are conducive to improving the natural frequency of the spirally corrugated tubes. The increase in the number of starts will also increase the internal stress of the spirally corrugated tubes and reduce the natural frequency. Therefore, under the interaction of the above factors, the natural frequency of the spirally corrugated tubes decreases first and then increases, the natural frequency of the four-start spirally corrugated tube is the smallest, and its first-order natural frequency is 174.7 Hz. The natural frequency of the eight-start spirally corrugated tube is the largest, and its first-order natural frequency is 230.55 Hz.

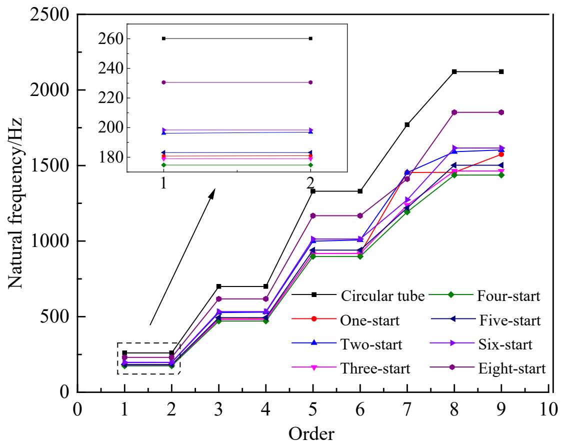

Fig. 3. Effect of the start value on the natural frequency of spirally corrugated tubes.

The first-order vibration mode of the spirally corrugated tube with 1-8 starts is shown in Fig. 4. Due to the fixed constraints imposed on both ends of the tube, the first-order maximum amplitude ($amplitude_{max}$) occurs at the center of the tube, and the $amplitude_{max}$ gradually decreases with the increase in the number of corrugated starts. The reason is that with the increase of the number of starts, the spirally corrugated tube will become thicker, and it is not easy to deform, so the $amplitude_{max}$ decreases. And the $amplitude_{max}$ of the spirally corrugated tube with 8 starts is 1.70 mm.

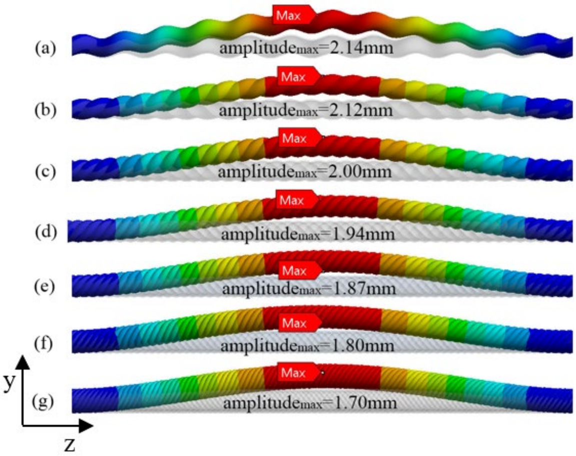

Fig. 4. Effect of the start value on the first-order vibration mode of spirally corrugated tubes.

3.2 Effect of Pitch

According to the results of Section 3.1, the natural frequency of the eight-start spirally corrugated tube is the largest. Therefore, the modal analysis of the eight-start spirally corrugated tubes (e/D_i=0.15, p/D_i=1.5-3) is carried out. The first nine natural frequencies are shown in Fig. 5, and the first-order modes are shown in Fig. 6. With the increase in pitch ratio, the degree of distortion of the spirally corrugated tubes decreases, resulting in a decrease in bending stiffness, which makes the spirally corrugated tubes more prone to bending deformation during vibration. Therefore, the natural frequency decreases, and the first-order $amplitude_{max}$ increases gradually. The natural frequency of the eight-start spirally corrugated tubes with a pitch ratio of 1.5 is the largest, and the first-order $amplitude_{max}$ is the smallest. The first-order natural frequency and the first-order $amplitude_{max}$ are 250.84 Hz and 1.61 mm, respectively.

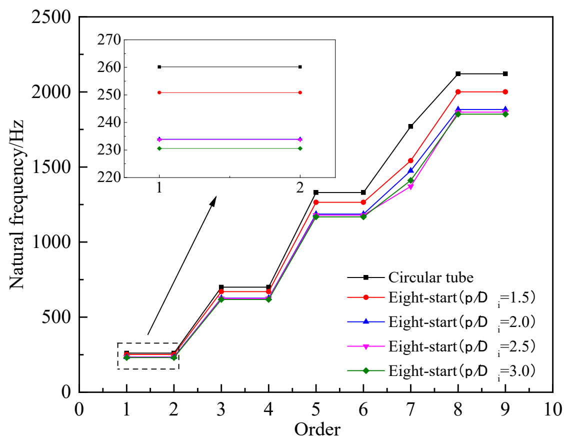

Fig. 5. Effect of the p/D_i on the natural frequency of spirally corrugated tubes.

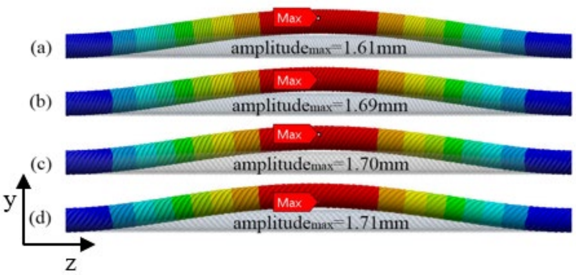

Fig. 6. Effect of the p/D_i on the first-order vibration mode of spirally corrugated tubes.

3.3 Effect of Corrugation Depth

Similarly, the modal analysis of the eight-start spirally corrugated tube (p/D_i=2.5, e/D_i=0.05-0.20) with different corrugation depths is carried out. The first nine natural frequencies are shown in Fig. 7, and the first mode shapes are shown in Fig. 8. With the increase in the corrugation depth ratio, the stiffness of the spirally corrugated tubes decreases. The larger corrugation depth means that the spirally corrugated tube is easier to bend and deform, thus reducing its overall stiffness. The decrease of stiffness means that the restoring force of the spirally corrugated tube becomes weaker and the response to the external force becomes softer. In addition, the increased corrugation depth will also increase the damping effect inside the spirally corrugated tubes. Damping can consume vibration energy, resulting in faster vibration attenuation. Therefore, the increase of the depth ratio will reduce the natural frequency and the first-order amplitude$_{max}$ of the spirally corrugated tubes. The natural frequency and the first-order amplitude$_{max}$ of the corrugation depth ratio of 0.05 are the largest, which are 247.28 Hz and 2.05 mm, respectively.

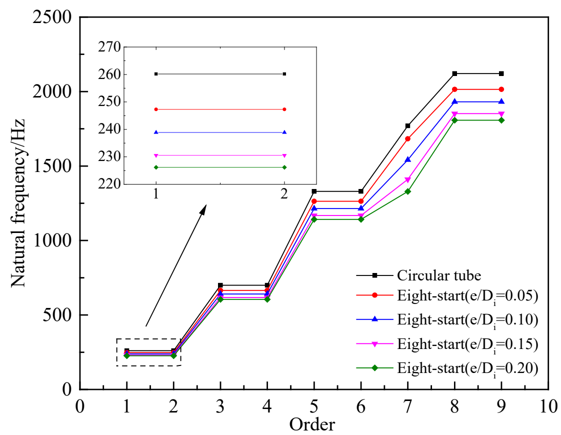

Fig. 7. Effect of the e/D_i on the natural frequency of spirally corrugated tubes.

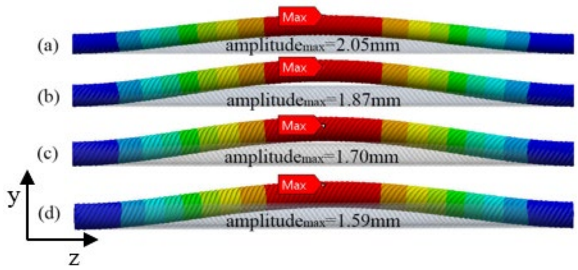

Fig. 8. Effect of the e/D_i on the first-order vibration mode of spirally corrugated tubes.

4. OPTIMAL DESIGN

In section 3, the influence of start value, pitch, and corrugation depth on the natural frequency of spirally corrugated tubes is studied. In order to quantitatively analyze the influence of each parameter on the natural frequency, a three-factor, four-level orthogonal test was used for research. The results are shown in Table 2. As shown in Table 2, the minimum first-order natural frequency occurs in the 8th group of tests (Start value:3, p/D_i=2.5, e/D_i=0.20), and its value is 148.86 Hz. The maximum first-order natural frequency occurs in the 16th group of tests (Start value:8, p/D_i=1.5, e/D_i=0.20), and its value is 254.29 Hz.

Table 2. Orthogonal test table

Num ber	(A) Start	(B) e/D_i	(C) p/D_i	(E) Error	First-order natural frequency/Hz
1	1	0.05	1.5	1	234.34
2	1	0.10	2.0	2	202.97
3	1	0.15	2.5	3	180.73
4	1	0.20	3.0	4	163.73
5	3	0.05	2.0	3	238.17
6	3	0.10	1.5	4	184.09
7	3	0.15	3.0	1	193.90
8	3	0.20	2.5	2	148.86
9	6	0.05	2.5	4	240.04
10	6	0.10	3.0	3	217.95
11	6	0.15	1.5	2	204.86
12	6	0.20	2.0	1	185.82
13	8	0.05	3.0	2	246.65
14	8	0.10	1.5	1	238.88
15	8	0.15	2.0	4	233.97
16	8	0.20	1.5	3	254.29

4.1 Range Analysis

The range analysis method has the advantages of simple calculation and intuitive results and is widely used in data analysis. The influence of start value, pitch, corrugation depth and first-order natural frequency is studied by range analysis. The results are shown in Table 3.

Table 3. Range analysis results

Parameters	First-order natural frequency/Hz			
	A	B	C	E
K_1[a]	781.77	959.20	877.58	852.94
K_2	765.02	843.89	860.93	803.34

K_3	848.67	813.46	822.23	891.14
K_4	973.79	752.70	808.51	821.83
k_1[b]	195.44	239.80	219.40	213.24
k_2	191.26	210.97	215.23	200.84
k_3	212.17	203.37	205.56	222.79
k_4	243.45	188.18	202.13	205.46
Range	52.19	51.63	17.27	21.95
Primary and secondary relationships	A>B>C			
Optimal combination	$A_4B_1C_1$			

[a] K: The sum of data for each factor and level

[b] k: The average value of data for each factor and level

In the test level range, the larger the first-order natural frequency of the target parameter is, the better it is. Therefore, the level that has a great influence on the first-order natural frequency should be selected, that is, the level corresponding to the maximum value of k_i in each factor. From the above data, it can be found that for the start value A: $k_4>k_3>k_1>k_2$, so the number of start is at the fourth level, the first-order natural frequency is the largest, and the number of start is 8. For the e/D_i factor B: $k_1>k_2>k_3>k_4$, so the first-order natural frequency is the largest under the first level of e/D_i, and e/D_i is 0.05. For the p/D_i factor C: $k_1>k_2>k_3>k_4$, it can be found that p/D_i has the largest first-order natural frequency under the parameters of the first level, and p/D_i is 1.5. Through the above analysis, it can be concluded that the optimized scheme is $A_4B_1C_1$, that is, the number of start is 8, e/D_i is 0.05, and p/D_i is 1.5. The optimized scheme is verified by experiments. It is found that the first-order natural frequency is 254.42 Hz under the conditions of 8 start value, 0.05 e/D_i, and 1.5 p/D_i, which is better than the best 254.29 Hz in Table 2. Therefore, this scheme is the best first-order natural frequency scheme.

4.2 Analysis of variance

The range analysis method can only judge the primary and secondary order of each factor and the combination of optimized parameters; it cannot judge the size of the error or the influence degree of each factor test result. Therefore, the variance analysis of the test results is carried out, and the results are shown in Table 4. Firstly, the significance levels of $\alpha=0.05$ and $\alpha=0.01$ were determined. When $P_i<0.01$, the influence of this factor on the test results is extremely significant; when $0.01<P_i<0.05$, it indicates that this factor has a significant effect on the test results; when $P_i>0.05$, it indicates that this factor has no significant effect on the test results. According to the results of variance analysis, for the first-order natural frequency $P_A < P_B < P_C$, it can be seen that the primary and secondary relationship of the influence degree of each parameter on the first-order natural frequency is: start value>e/D_i >p/D_i, which is consistent with the results of range analysis. The P values are all greater than 0.05, indicating that the influence of the first-order natural frequency is not significant.

Table 4. Analysis of variance results

Source of variance	Sum of squares of deviations	Free degree	Mean square	F	P	Significance
A	6741.6	3	2247.2	6.080	0.086	P>0.05
B	5632.0	3	1877.3	5.079	0.107	P>0.05
C	784.1	3	261.4	0.707	0.609	P>0.05
E	1108.9	3	369.6			

5. CONCLUSIONS

In this paper, the modal analysis of spirally corrugated tubes is carried out by the numerical method. The influence of the number of starts, pitch p, and corrugated depth D_i on the vibration characteristics of spirally corrugated tubes is studied. Based on the orthogonal test method, the influence of each parameter on the natural frequency of spirally corrugated tubes is studied. The specific conclusions are as follows:

(1) Due to the symmetry of the geometric structure of the tube bundle, the natural frequencies of the first and second orders, the third and fourth orders, and the fifth and sixth orders are equal to each other. With the increase in the number of starts, the natural frequency of the spirally corrugated tubes decreases first and then increases, and the natural frequency of the four-start spirally corrugated tubes is the smallest. With the increase in pitch and corrugation depth, the natural frequency of the spirally corrugated tube decreases.

(2) The first-order amplitude$_{max}$ of the spirally corrugated tube occurs at the center of the tube, and the first-order amplitude$_{max}$ gradually decreases with the increase in the number of starts and the corrugation depth ratio. As the pitch ratio increases, the first-order amplitude$_{max}$ also increases.

(3) The number of starts is the main factor affecting the natural frequency of the spirally

corrugated tubes. In the parameter range of this study, the natural frequency of the spirally corrugated tubes with eight starting points (p/D_i=1.5, e/D_i=0.05) is the largest, and its first-order natural frequency is 254.42 Hz.

ACKNOWLEDGMENT

Financial support for this work was provided by the National Natural Science Foundation of China (No. 22068024).

REFERENCES

Ashley, H. and Haviland, G., “Bending vibrations of a pipe line containing flowing fluid,” J. Appl. Mech., Vol. 17, No. 3, pp. 229-232 (1950).

Bergles, A. E., “Some Perspectives on Enhanced Heat Transfer—Second-Generation Heat Transfer Technology,” J. Heat Transfer, Vol. 110, No. 4b, pp. 1082-1096 (1988).

Fan, S. J. and Yang, C., “Numerical Calculation of Fluid-Structure Coupling Vibration of a Water Pipeline,” Noise Vib., Control, Vol. 30, No. 6, pp. 43-46 (2010).

Ghadirian, H., Mohebpour, S., Malekzadeh, P., and Daneshmand, F., “Nonlinear free vibrations and stability analysis of FG-CNTRC pipes conveying fluid based on Timoshenko model,” Compos. Struct., Vol. 292 (2022).

Guo, J., Yan, Y. X., Liu, W., Jiang, F. M., and Fan, A. W., “Effects of upwind area of tube inserts on heat transfer and flow resistance characteristics of turbulent flow,” Exp. Therm. Fluid Sci., Vol. 48, No. 7, pp. 147-55 (2013).

Hou, Q., Ren, J., and Gu, M., “Analysis of behaviour of axial vibration of buried pipelines by travelling wave method,” J. Tongji Univ. Vol. 37, No. 5, pp. 618-622 (2009).

Ji, J. D., Ge, P. Q., and Bi, W. B., “Numerical analysis of shell-side flow-induced vibration of elastic tube bundle in heat exchanger,” J. Hydrodyn., Vol. 107, pp. 544-551 (2018).

Ji, J., Deng, X., Zhang, J., Li, F., and Zhou, R., “Study on Vibration and Heat Transfer Performances of a Modified Elastic Tube Bundle Heat Exchanger,” Journal of Physics: Conference Series (2022).

Jin, Z. J., Liu, B. Z., Chen, F. Q., Gao, Z. X., Gao, X. F., and Qian, J. Y., “CFD analysis on flow resistance characteristics of six-start spirally corrugated tube,” Int. J. Heat Mass Transfer, Vol. 103, pp. 1198-207 (2016).

Ke, Y., Ge P.Q., Bi, W.B., Su, Y.C., and Hu, R.R., “Vibration characteristics of fluid-structure interaction of conical spiral tube bundle,” J. Hydrodyn., Vol. 22, No. 1, pp. 121-128 (2010).

Kongkaitpaiboon, V., Promthaisong, P., Chuwattanakul, V., Wongcharee, K., and Eiamsa-ard, S., “Effects of spiral start number and depth ratio of corrugated tube on flow and heat transfer characteristics in turbulent flow region,” J. Mech. Sci. Technol., Vol. 33, No. 8, pp. 4005-4012 (2019).

Lee, U. and Park, J., “Spectral element modelling and analysis of a pipeline conveying internal unsteady fluid,” J. Fluid Struct., Vol. 22, No. 2, pp. 273-292 (2006).

Li, F., Jing, C., Duan, M., Chen, A., and Jian, S., “Two-phase Flow Induced Vibration of Subsea Span Pipeline,” International ocean and polar engineering conference (2016).

Liu, T., and Li, Z. M., “Nonlinear vibration analysis of functionally graded material tubes with conveying fluid resting on elastic foundation by a new tubular beam model,” Int. J. Non-Linear Mech., Vol. 137 (2021).

Navaei, A. S., Mohammed, H. A., Munisamy, K. M., Yarmand, H., and Gharehichani, S., “Heat transfer enhancement of turbulent nanofluid flow over various types of internally corrugated channels,” Powder Technol., Vol. 286, pp. 332-341 (2015).

Omidi, M., Farhadi, M., and Darzi, A.A.R., “Numerical study of heat transfer on using lobed cross sections in helical coil heat exchangers: Effect of physical and geometrical parameters,” Energ. Convers. Manage., Vol. 176, pp. 236-245 (2018).

Peng, H., Zhang, H., and Qi, Z., “Frequency-spectrum Characteristic Analysis and Structure Parameters Optimization of TBM Hydraulic Pipelines,” Noise Vib. Control, Vol. 35, No. 1, pp. 58-62 (2015).

Qu, W., Zhang, H., Li, W., and Peng, L., “Dynamic characteristics of a hydraulic curved pipe subjected to random vibration,” Int. J. Pressure Vessels Piping, Vol. 193, No. 104442 (2021).

Wang, X. and Lambert, S. B., “Stress intensity factors and weight functions for longitudinal semi-elliptical surface cracks in thin pipes,” Int. J. Pressure Vessels Piping, Vol. 65, No. 1, pp. 75-87 (1996).

Wang, Z., Zhou, Z. J., Lu, H., Wen, Z. J., and Xia, Y. M., “Coupling Model Analysis on Fluid Structure Interaction in Lifting Pipeling Based on ADINA.” Adv. Mater. Res., Vol. 468-471, pp. 238-244 (2012).

Wu, G.X., Zhao, X., Shi, D., and Wu, X., “Analysis of Fluid–Structure Coupling Vibration Mechanism for Subsea Tree Pipeline Combined with Fluent and Ansys Workbench,” Water, Vol. 13, No. 7 (2021).

Wu, J., Li, C. J., Zheng, S. Y., and Gao, J. H., “Study on Fluid-Structure Coupling Vibration of Compressor Pipeline,” Shock Vib., pp. 1-12

(2019).

Wu, Z.W., Qian, C.F., Liu, G., Liu, Z.S., and Shen, P., "Mechanical Properties and Heat Transfer Performance of Conically Corrugated Tube," Materials, Vol. 14, No. 17 (2021).

Yang, S., Zhang, L., and Xu, H., "Experimental study on convective heat transfer and flow resistance characteristics of water flow in twisted elliptical tubes," Appl. Therm. Eng., Vol. 31 No. 14-15, pp. 2981-2991 (2011).

Zhang, L. N., Zhao, H., and Liu, M. S., "Research on Fluid-Structure Interaction Dynamic Characteristics of Steam Generator Heat Exchanger Tubes," Adv. Mater. Res., Vol. 482-484, pp. 183-187 (2012).

Zhou, Z. J., Hao, L. U., Wang, Z., and Zuo, M. J., "Characteristics Analysis on Considering Fluid-Solid Coupling Effects for Vertical Lifting Pipe," Period. Ocean Univ. China, (2013).

NOMENCLATURE

β spiral angle

$amplitude_{max}$ maximum amplitude

A cross-sectional area

C wetting perimeter

D_i inner diameter

e corrugated depth

p pitch

螺旋波紋管模態分析與優化設計

潘闖 唐慶慶 戴源德
南昌大學先進製造學院

摘 要

螺旋波紋管是一種高效換熱管，有製造簡單、成本低、雙向強化傳熱等優點，而管束結構的抗振性是保證其換熱的基礎。因此，選擇等效內徑的螺旋波紋管作為研究對象，採用數值類比的方法對其進行了模態分析，研究了波紋起點數、螺距與波紋深度對螺旋波紋管振動特性的影響。結果表明：隨著起點數的增加，螺旋波紋管的固有頻率也隨之增大；隨著螺距與波紋深度的增大，螺旋波紋管的固有頻率逐漸減小。此外，由於換熱管在換熱器中的低頻環境下更易發生共振現象，造成疲勞失效。因此，以螺旋波紋管的一階固有頻率作為目標參數，對多起點螺旋波紋管進行優化設計，得到了抗振性最好的螺旋波紋管結構參數。